Chemosphere 365 (2024) 143329

Contents lists available at ScienceDirect

Chemosphere

journal homepage: www.elsevier.com/locate/chemosphere

Influence of carbon content and irradiation modes on the antibiotic removal from water using VIS-activated TiO_2/expanded graphite composite photocatalysts

Rodrigo Teixeira Bento [a,*], Priscila Hasse Palharim [b], Antonio Carlos Silva Costa Teixeira [b], Marina Fuser Pillis [a]

[a] Nuclear and Energy Research Institute, IPEN–CNEN/SP, University of São Paulo, Lineu Prestes Avenue 2242, São Paulo, SP, Brazil
[b] Research Group in Advanced Oxidation Processes (AdOx), Department of Chemical Engineering, Escola Politécnica, University of São Paulo, Av. Prof. Luciano Gualberto, tr. 3, 380, São Paulo, SP, Brazil

HIGHLIGHTS

- Photoefficient TiO_2/C films were deposited on glass substrates by cold spray coating.
- Morphological/structural changes and type-II heterojunction formation were observed.
- The films showed good reusability on the SDZ degradation over 4 photocatalytic cycles.
- The influence of irradiation modes and role of oxidizing species were discussed.
- Irradiation mode effect and photocatalytic mechanism of SDZ by TiO_2/C were proposed.

GRAPHICAL ABSTRACT

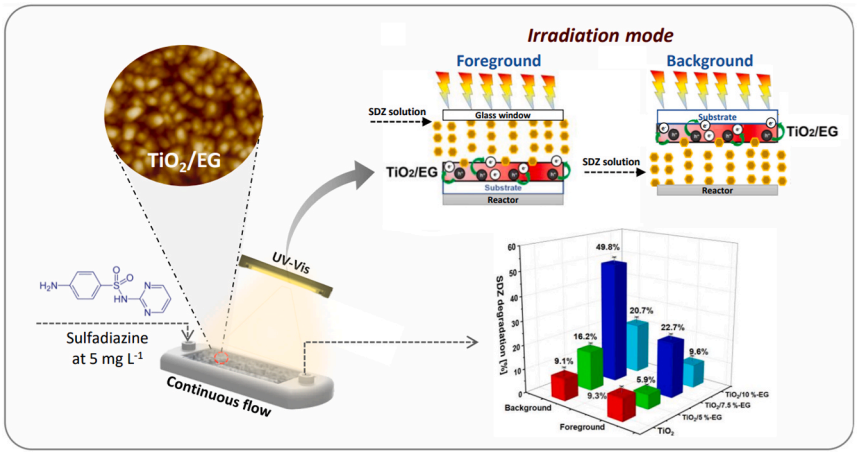

ARTICLE INFO

Handling editor: Vicente Rodríguez-González

Keywords:
Expanded graphite
TiO_2
Heterojunction
Photocatalysis
Photodegradation

ABSTRACT

TiO_2/expanded graphite (TiO_2/EG) composite films were applied to water treatment for sulfadiazine (SDZ) degradation in a continuous flat plate photochemical reactor. The films were synthesized by sol-gel method and deposited on borosilicate glass by airbrush spray coating technique, forming a TiO_2/C heterojunction. Increasing the amount of carbon promoted more efficient photocatalytic removal of SDZ under simulated sunlight, which increased from 9.1% in the absence of carbon to 49.8% for the material containing 7.5% C. From the formation of the TiO_2/C heterojunction, morphological modifications, changes in the electronic structure and reduction of the band gap energy were observed. Type-II heterojunction formation was observed. Foreground and background irradiation modes were investigated, and a possible photocatalytic mechanism was proposed. TiO_2/7.5 %-EG exhibited the best photocatalytic performance, with the possibility of reuse. The films showed good reusability in

* Corresponding author.
E-mail address: rodrigo.bento@ipen.br (R.T. Bento).

https://doi.org/10.1016/j.chemosphere.2024.143329
Received 20 April 2024; Received in revised form 21 August 2024; Accepted 10 September 2024
Available online 11 September 2024

the SDZ degradation over 4 photocatalytic cycles. The influence of irradiation modes and the role of oxidizing species were discussed. The results showed that TiO_2/EG hybrid films are a promising alternative for practical photocatalytic applications under sunlight.

1. Introduction

Titanium dioxide (TiO_2) is one of the most widely used semiconductor materials as catalytic films for water and effluent treatment processes via heterogeneous photocatalysis, primarily due to its high efficiency, photo stability, and physicochemical properties (Bento et al., 2019; Temam et al., 2022). Nevertheless, TiO_2 presents limitations regarding its photocatalytic efficiency when used under visible light irradiation, since it exhibits low photon absorption above 390 nm (De Araujo Gusmão et al., 2022; Bento et al., 2021a; Reza et al., 2017). To overcome this limitation, the combination of TiO_2 with other materials is considered a promising approach, among which the formation of heterojunctions is notable (Duoerkun et al., 2020; Wannapop and Somdee, 2022). Photocatalytic heterojunctions are systems of two or more different semiconductors that interface with each other (Li et al., 2018; Bento et al., 2022). The use of photocatalytic heterojunctions has proven to be an effective strategy to improve light absorption, the generation of highly active radicals such as $O_2^{\bullet -}$ and $HO^{\bullet}$, and consequently, the behavior of the photocatalyst under visible light (Murugan et al., 2021).

Several studies have highlighted the importance of using photocatalytic heterojunctions due to their high potential to solve environmental and technological problems (Palharim et al., 2022; Li et al., 2023; Aouf et al., 2023). Among the different types of existing heterojunctions, the combination of TiO_2 with carbon-based materials (e.g. graphene, graphene oxide, expanded graphite) stands out, since it combines the optical and electronic properties of carbon with the photocatalytic properties of a semiconductor material (Tang et al., 2018; Tismanar et al., 2021). This system has been studied due to its high photocatalytic efficiency and its ability to be produced in an affordable and environmentally friendly manner. TiO_2/C composite photocatalysts have been widely used for the removal of organic pollutants from water, such as dyes, pesticides and alcohols, and also in environmental protection applications, for example, in landfill odor control and neutralizing toxic gases (Bento et al., 2022).

Zhang et al. (2022) synthesized photocatalysts composed of TiO_2 doped with graphitic carbon (TiO_2-GC) via the impregnation method, thus combining the advantages of both materials; the composites were investigated in the synergetic adsorption-photodegradation tetracycline antibiotics. Structure characterization confirmed the formation of the Ti–*O*–C valence bond, with a decrease in bandgap energy to 2.67 eV. Compared with pure TiO_2, the TiO_2-GC photocatalyst exhibited exceptional morphological characteristics, good reusability, and high photocatalytic performance, with94% tetracycline removal under visible light.

Zhang et al. (2020) proposed a novel photodegradable nano--graphite/TiO_2 composite film for the degradation of PVC (polyvinyl chloride) plastic under visible light. The results showed that the composite film produced in this study represents a viable and efficient solution for addressing the "white pollution" issue, with an excellent photodegradability of about 62%. Wu et al. (2021) investigated the photoactivity of the V_2O_5–MoO_3/TiO_2-expanded graphite (EG) catalysts on the NH_3 reduction. The high shear method achieved a homogeneous distribution of TiO_2 particles with EG.

In turn, in our previous study (Bento et al., 2022), TiO_2/expanded graphite (TiO_2/EG) films were obtained by sol-gel spray coating method to evaluate the decolorization of methyl orange dye under visible light. EG nanosheets were synthesized directly from bulk graphite by UVC-assisted liquid-phase exfoliation technique (LPE) without the addition of aggressive oxidizing agents, which characterizes the process as eco-friendly. The formation of the TiO_2/C heterojunction resulted in morphological modifications, changes in the electronic structure, and a broadening of the light absorption range, which favored its photocatalytic efficiency.

Therefore, it is noted that TiO_2/C heterojunctions have great potential in water treatment and environmental protection applications. However, it is important to highlight that there are still few studies aimed at understanding the photocatalysis mechanisms involved in these composites, as well as developing strategies to further improve their efficiency. To shed light on this topic, in this research TiO_2/EG films were synthetized by sol-gel method, and deposited on borosilicate glass substrates by a simple cold spray coating technique to evaluate their photocatalytic behavior in the degradation of the antibiotic sulfadiazine, selected as a model contaminant of environmental concern, under UV–Vis irradiation. The effects of irradiation pathways and carbon concentration on the morphological and structural characteristics of the composite films are presented and discussed. The explanation on the degradation mechanism of SDZ when the composite film is foreground and background illuminated, as well as the possible degradation pathways of SDZ by UV–Vis-active TiO_2/EG photocatalysts were proposed.

2. Experimental

2.1. Expanded graphite nanosheets

Expanded graphite (EG) nanosheets were produced by UVC-assisted liquid phase exfoliation technique using natural graphite (Quimidrol Com. Ind. LTDA) as carbon precursor, as previously described by Bento et al. (2022). A dispersion of 0.6 g of graphite in a solution of deionized water, acetone and isopropyl alcohol was irradiated with UVC light (λ = 253.7 nm, OSRAM Licht AG, Puritec 9 W) at room temperature for 2 h. Previous studies suggested the influence of the graphite exfoliation time on the photocatalytic activity of TiO_2/EG, and the existence of an optimal time at which the hybrid photocatalyst exhibits better performance (Bento et al., 2022).

2.2. TiO_2/EG composite films

Hybrid TiO_2/EG films with a thickness of 300 nm were obtained by the sol-gel method. Preliminary investigations suggested the existence of an optimal thickness in which TiO_2 films exhibit optimal photocatalytic efficiency (Bento et al., 2019, 2021b; Marcello et al., 2020). The sol-gel composite was prepared using 5 mL of titanium(IV) isopropoxide (TTiP, $Ti(OCH(CH_3)_2)_4$, 97%, Sigma-Aldrich) dissolved in 50 mL of isopropanol. Expanded graphite was added to the solution at 5, 7.5 and 10 % (w:v). Then, 1.5 mL of sulfuric acid (H_2SO_4) was added to reach pH = 3. The solution was stirred at 75 °C for 60 min. Next, the composite films were deposited on borosilicate glass substrates (25 × 76 × 1 mm) by a low-cost cold spray coating technique employing an airbrush. The solution was sprayed onto the substrates at a scanning speed of approximately 17 mm s^{-1}. Subsequently, the samples were dried at 100 °C for 60 min, and heat treated at 550 °C for 30 min.

2.3. Characterization

X-ray diffraction (XRD) analysis was performed using a Rigaku Multiflex instrument, with monochromated CuKα radiation, at an incidence angle of 5°, a scanning rate of 0.02°, and a 2θ range from 5 to 80°. Atomic force microscopy (AFM) was used in tapping mode with a SPM Bruker NanoScope IIIA instrument. AFM scan size images of 2 μm × 2

μm were taken at a frequency of 0.9 Hz. Raman spectroscopy was used with a WITEC Raman Microscope Alpha300 R instrument, exposure time of 30 s, $\lambda = 532$ nm, and a range of 100 cm^{-1} to 3500 cm^{-1}. The films surface was cleaned with deionized water prior to analysis (Bento et al., 2021a, 2021b). The band gap energy (E_g) of the films were estimated by the Tauc method (Bento et al., 2022), using a Shimadzu UV–Vis spectrophotometer equipment (UV–1650PC model, 300 nm $\leq \lambda \leq$ 1100 nm, 1-nm step). X-ray photoelectron spectroscopy (XPS) (Thermo Scientific K-Alpha, with resolution of 0.1 eV, and 400-μm spot size beam) was applied to evaluate the chemical states on the surface of the films.

2.4. Photocatalytic activity assays

The photocatalytic activity of the synthesized composite films was evaluated using sulfadiazine (SDZ) as a model pollutant. Sulfadiazine ($C_{10}H_{10}N_4O_2S$, CAS 68-34-9, HPLC standard, ≥99 %) was acquired from Sigma-Aldrich. Photocatalytic experiments were performed in a 3.0 mL continuous flat plate microstructured photochemical reactor, prototyped by additive 3D printing, with a 25 × 76 mm borosilicate glass irradiation window, as described elsewhere (Ramos et al., 2021). Fig. 1 shows the schematic diagram of the photocatalytic apparatus. Photocatalytic experimental parameters, such as pH medium and initial pollutant concentration were established from previous studies (Lastre-Acosta et al., 2015; Rivas-Ortiz et al., 2017). The experiments were carried out by varying the face of the film to be irradiated, i.e., foreground or background (Fig. 1). When the films were irradiated on the front face (foreground), the 4.8 cm-long film was positioned at the bottom of the reactor, which was closed at the top with a borosilicate glass window and sealed; for background irradiation (through the substrate), the sample was positioned at the top of the reactor in such a way that the deposited material was in contact with the solution inside the reactor, and the window was sealed.

60 mL of SDZ solution at 5-mg L^{-1} initial concentration, pH around 6 (without adjustment), was loaded into a syringe coupled with a precision syringe pump (11 Elite, Harvard Apparatus Ltd. Holliston, MA, USA) used to feed the reactor. The SDZ solution was fed into the reactor at a volumetric flow rate of 10.0 mL h^{-1} for 45 min under dark conditions. Then, the reactor was fed at a flow rate of 1.5 mL h^{-1}, to obtain a residence time of 120 min, and exposed to UV–Vis radiation provided by a high-power HgI_2 lamp (400W HPI-T, Phillips Co.) mounted on a parabolic reflector and positioned 15 cm from the top of the reactor; the UV-A irradiance (300–400 nm) reaching the reactor was measured by a spectroradiometer (Luzchem, SPR-4002) to be ~4.6 mW cm^{-2}, equivalent to the output of the standard AM 1.5G solar spectrum at sea level (Gueymard, 2004). The photocatalytic experiments were repeated thrice for each condition. The reusability of the film was also evaluated for four photocatalytic cycles of 120 min of space time each. The possibility of reuse of the supported photocatalysts is an important requirement for the real-world application of heterogeneous photocatalysis in water treatment.

Samples of 200 μL were collected at the reactor outlet at steady-state and analyzed by high-performance liquid chromatography (HPLC), using a Shimadzu LC20 HPLC chromatograph equipped with a C18 column (Prominent) and a UV–Vis detector (SPD20A). The mobile phase was methanol:water (25:75), with a flow rate of 1.0 mL min^{-1}, injection volume of 50 μL, and oven temperature of 35 °C. The retention time was about 8 min and the detection wavelength was 243 nm. The limit of detection of SDZ was 0.11 mg L^{-1}, and the limit of quantification was 0.33 mg L^{-1}.

2.5. Effect of scavengers

The role of oxidizing species was investigated through additional experiments using radical scavengers, in order to deeply understand the photocatalytic degradation mechanism of SDZ under simulated sunlight. These experiments were performed using formic acid, 1,4-hydroquinone, potassium iodide (KI), tert-butanol (TBA) and sodium azide as scavengers at an initial concentration of 0.02 mol L^{-1} each (Palharim et al., 2022). All experiments were performed with the TiO_2/7.5 %-EG photocatalyst, which showed the best photocatalytic activity.

3. Results and discussion

3.1. XRD characterization

TiO_2/EG was investigated by XRD, as shown in Fig. 2. The phases formed were identified with the JCPDS (Joint Committee on Powder Diffraction Standards) database. The composite films showed the anatase-TiO_2 phase (JCPDS 21–1272) (Bento et al., 2022; Tismanar et al., 2021; Marcello et al., 2020). The results suggest that the TiO_2/EG films exhibited the same characteristic peaks after the addition of expanded graphite. The crystallite size values were estimated from the Scherrer equation (Marcello et al., 2020). It was observed that the composite films exhibited crystallite size values of 15.9 nm (5 %-EG), 13.2 nm (7.5 %-EG), and 11.8 nm (10 %-EG). The mean crystallite size values of the TiO_2/C composite films are lower when compared to pure TiO_2 (17.5 nm), and the lower intensities of the TiO_2 peaks observed in the diffractogram for samples containing expanded graphite and specially for that of 10 % EG sample is ascribed to the incorporation of carbon into the TiO_2 lattice (Samet et al., 2013; Liu et al., 2005). The

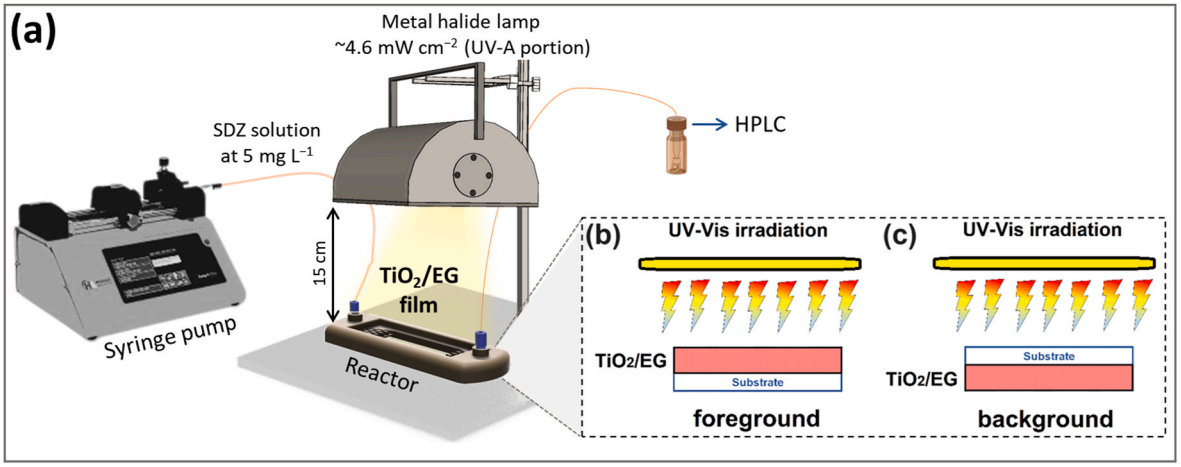

Fig. 1. (a) Schematic diagram of the photocatalytic apparatus applying the TiO_2/EG composite films to sulfadiazine removal under different UV–Vis irradiation modes: (b) Foreground (front catalyst surface) and (c) Background (through the borosilicate glass substrate).

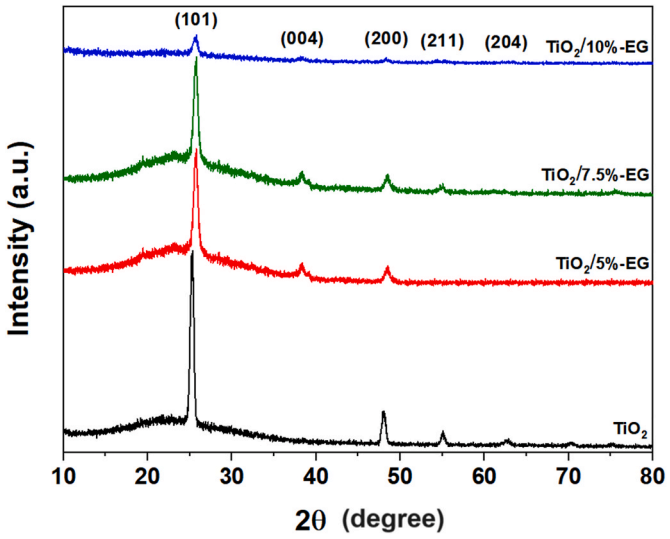

Fig. 2. XRD patterns of TiO_2 and TiO_2/EG composite films, obtained by spray coating technique at 550 °C, with different carbon contents.

presence of expanded graphite exerts an inhibitory effect on the crystallization kinetics and grain growth of TiO_2 (Guan et al., 2023). No diffraction peaks were observed for carbon species, such as graphene, graphene oxide (GO) or graphite oxides – a trend similar to that of other studies (Khalid et al., 2018; Wu et al., 2015; Jia et al., 2016; Jiang et al., 2011). Furthermore, a slight shift of the peaks was observed after the addition of carbon, which may be due to the formation of the TiO_2–C heterojunction that promotes distortions in the crystal lattice of the semiconductor.

3.2. AFM images

Fig. 3 shows AFM images of the surface topography of the pure TiO_2 films and TiO_2/EG composite films heat-treated at 550 °C. The presence of exfoliated graphite promoted significant surface modifications in the films, such as roughness and grain size, which may provide the formation of morphological characteristics favorable for their photocatalytic application (Bento et al., 2021b; Guan et al., 2016). All composite films are formed by small spherical grains in the range of 41–50 nm and exhibited morphological homogeneity.

The variation of the root mean square (RMS) roughness from 8.4 nm, corresponding to pure TiO_2 (Fig. 3a), to about 5~7 nm of the composite films (Fig. 3b–d), reveals the influence of carbon content on the surface

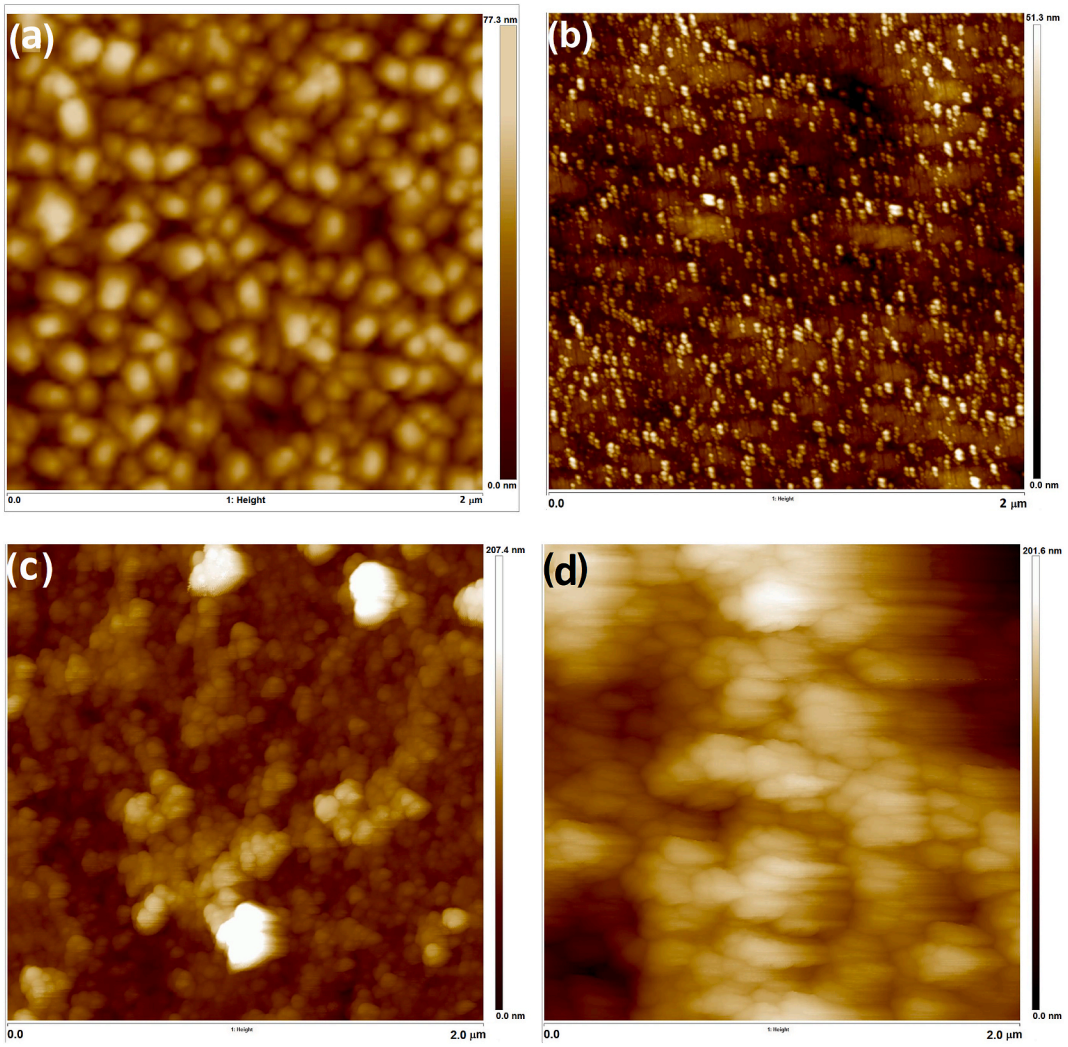

Fig. 3. AFM images of the surface topography of the (a) pure TiO_2 film, and the TiO_2/EG composite films at different carbon contents (b) 5%, (c) 7.5%, and (d) 10%. The films were obtained by sol-gel method, deposited on borosilicate glass substrates by cold airbrush spray coating technique at room temperature, and heat-treated at 550 °C.

characteristics of the hybrid photocatalysts, as described in the literature (Bento et al., 2022; Tismanar et al., 2021). The values of mean grain size and surface roughness of the films can be seen in Table 1.

The results can be explained by assuming that EG interacts with TiO_2 nanoparticles in a stable manner and leads to the formation of more compact and thicker aggregates. Karthik et al. (2020) also reported the formation of hybrid films with surfaces of similar roughness. The authors suggest that the more protruding agglomerates are a fraction of the EG nanosheets clustered on the film surface. Roughness is an important morphological characteristic related to the grain size distribution on the film surface, which consequently influences the contact of the photocatalyst with the adsorbed pollutant particles, as well as with the photons emitted by the light source (Bento et al., 2019, 2022).

3.3. Raman spectroscopy

The Raman spectroscopy technique can be used to demonstrate the effects of C content on the crystal structure of the hybrid photocatalysts. For the vibrational signals in the TiO_2 region (Fig. 4a), the Raman spectra of the films indicate peaks at 144, 197, 397, 515 e 639 cm^{-1}, which can be assigned to the vibration modes of the anatase-TiO_2 phase (Bento et al., 2022; Zabihi et al., 2017). No peaks related to the rutile-TiO_2 phase were found. Simultaneously, for the vibrational signals of the C region (Fig. 4b), the Raman spectra of the films indicate peaks corresponding to D, G and 2D bands – signals characteristic of exfoliated carbon-based materials (Jiang et al., 2011; Xue et al., 2017) – respectively located at 1353, 1578 and 2700 cm^{-1}. It is observed that the G and 2D peaks show a slight shift of 4 cm^{-1} and 19 cm^{-1}, respectively, as the C content increases. Such observed behavior may be associated with the formation of the semiconductor-C heterojunction by the Ti–C and Ti–*O*–C bonds (Bento et al., 2022; Wu et al., 2015; Liu et al., 2014).

A significant reduction of the I_D/I_G intensity ratio is also observed, as shown in Table 1. I_D/I_G ratio allows analyzing the proportion of sp_3 defect domains and the crystallinity degree of the films by the presence of sp^2 domains. The ratios for TiO_2/5 %-EG, TiO_2/7.5 %-EG and TiO_2/10 %-EG are 1.26, 1.17 and 1.13, respectively. The results indicate that TiO_2/EG contains a larger number of sp^2 domains in accordance with the increase in the amount of carbon, as also observed by Wu et al. (2015). The free electrons of the C sp^2 hybridization can form a large π-conjugative system, and act as fast conduction electrons – which can favor the formation of highly oxidizing species and hance the photocatalytic performance of the composite films (Wu et al., 2015).

3.4. UV–vis spectrophotometry

The UV–Vis absorption spectra of the TiO_2 and TiO_2/EG films were used to estimate the band gap energies (E_g) of the TiO_2 film and the TiO_2/EG composite films (Table 1). As shown in Fig. 5, the pure TiO_2 film exhibited an E_g value of about 3.2 eV, similar to that observed in the literature for the anatase-TiO_2 phase (De Araujo Gusmão et al., 2022; Tismanar et al., 2021). In the presence of expanded graphite, the E_g values were significantly reduced to less than 2.8 eV. The results suggest that the structural changes promoted the reduction of the band gap of the semiconductor and subsequently improved the absorption of photons with lower energy to activate the photocatalyst under visible light.

The band gap reduction of photocatalysts may be impacted by the heat-treatment temperature and the carbon amount, which are intrinsically related to the semiconductor crystalline structure (Samet et al., 2013; Liu et al., 2005). After the heat treatment, rearrangements occur in the crystalline lattice of the photocatalyst, which can influence its electronic characteristics. This phenomenon can stem from the mitigation of structural imperfections, resulting in enhanced crystalline alignment and reduced defect density, as well as the enhancement in the electronic states dispersion within the semiconductor, thereby potentially influencing the reorganization of the energy level (Guan et al., 2023).

Table 1
Morphological characteristics and structural properties of the TiO_2 and TiO_2/EG composite films obtained by spray coating method, with different amounts of carbon.

	Mean grain size (nm)	RMS roughness (nm)	I_D/I_G	Band gap energy (eV)
TiO_2	76.1 ± 8.4	8.4	–	3.2
TiO_2/5 % - EG	41.3 ± 5.3	5.1	1.26	2.8
TiO_2/7.5 % - EG	49.8 ± 9.8	7.2	1.17	2.6
TiO_2/10 % - EG	44.5 ± 6.9	6.8	1.13	2.1

3.5. XPS measurements

High resolution XPS spectra of C1s (Fig. 6a) and O1s XPS (Fig. 6b) were obtained to evaluate the chemical state of the species formed on the films surface. The C1s peak at 284.8 eV was set as a reference (Bento et al., 2021b). After carbon addition, the results evidenced the presence of peaks characteristic of Ti–C (283 eV) and Ti–*O*–C (534 eV) bonds – an effect that supports the formation of the TiO_2–C heterojunction, also observed in previous studies (Ali et al., 2022; Sun et al., 2013; Akhavan and Ghaderi, 2009; Vallejo et al., 2019). Peaks are also observed at 284 eV (C–C), 285 eV (C–O), 287 eV (C(O)OH) and 288 eV (C═O), in the C1s region, as well as peaks at 529 eV (Ti–*O*–Ti) and 531 eV (HO^-), in the O1s region. These bonds are typical of TiO_2 and TiO_2/C materials (Bento et al., 2019; Ali et al., 2022; Sun et al., 2013). Tang et al. (2018) and Sun et al. (2013) suggested that the ability to absorb photons in the visible light region is mainly related to the formation of Ti–C and/or Ti–*O*–C bonds, which can promote the formation of intermediate energy states, thus favoring the reduction of the band gap energy, in agreement with the trend observed here. The heat treatment after the TiO_2-EG film deposition favors the carbon insertion into the TiO_2 lattice, which promotes intermediate energy states between conduction band (CB) and valence band (VB) (Guan et al., 2023).

3.6. Photocatalytic experiments

TiO_2 and TiO_2/EG films were evaluated for their photoactivity for sulfadiazine (SDZ) degradation under simulated sunlight irradiation, in a continuous flat-plate photochemical reactor. The photocatalytic experiments were conducted by irradiating the background (substrate) and foreground (surface) of the films. For the calculation of the specific degradation rate, it was assumed that the reactor can be described by a plug flow model (PFR). In that case, the molar balance for SDZ (Levenspiel, 2013) is given by Eq. (1), where F_{SDZ} is the molar flowrate of SDZ (mol h^{-1}), V is the volume of the reactor (L), and r is the degradation rate.

$$\frac{dF_{SDZ}}{dV} = -r_{SDZ} \tag{1}$$

Considering that the reaction proceeds with pseudo-first order kinetics, where $r_{SDZ} = -k'C_{SDZ}$, Eq. (1) results in Eq. (2):

$$k' = -\frac{F_{SDZ,0}}{V \times C_0}\int_0^{X_{SDZ}} \frac{dX_{SDZ}}{(1-X_{SDZ})} \tag{2}$$

where k' corresponds to the pseudo-first order degradation rate constant (h^{-1}), C_0 is the inlet SDZ concentration (mol L^{-1}), and X_{SDZ} is the steady-state conversion. Solving the definite integral leads to Eq. (3), where Q is the liquid flow rate (L h^{-1}).

$$k' = \frac{Q}{V} ln(1 - X_{SDZ}) \tag{3}$$

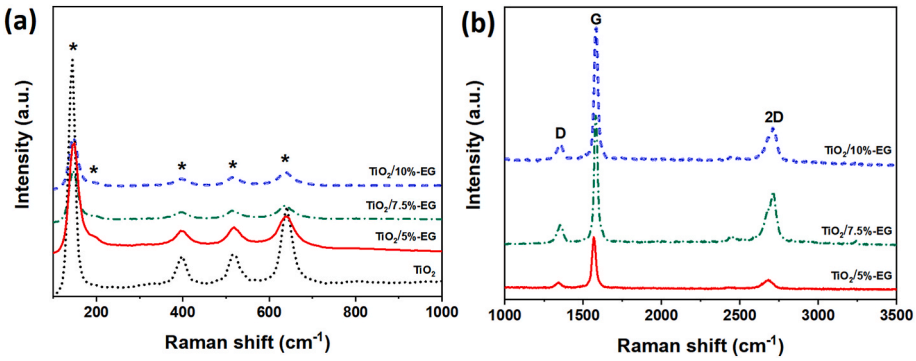

Fig. 4. Raman spectra of the TiO_2 and TiO_2/EG films obtained by spray coating at 550 °C: (a) TiO_2 peak signal region and (b) Carbon peak signal region.

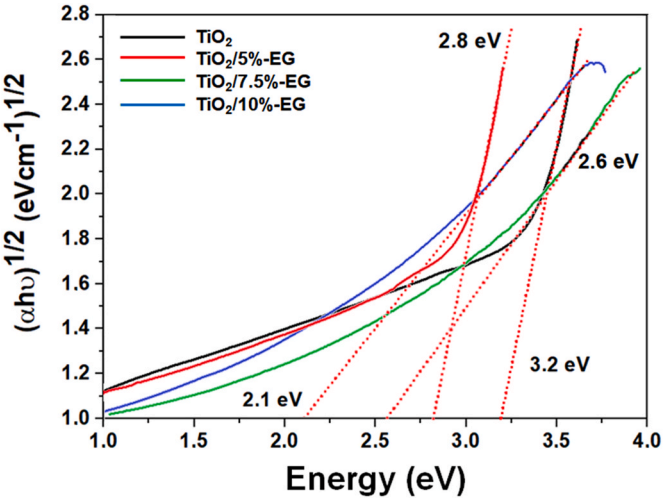

Fig. 5. Estimated band gap energies of TiO_2 and TiO_2/EG films with different carbon contents.

Fig. 7 and Table 2 summarize the main results. Experiments carried out under dark conditions showed steady-state removals of SDZ of less than 10% by adsorption for all synthesized films. Photolysis control was realized as described on previous work (Lastre-Acosta et al., 2021). The pure TiO_2 photocatalyst showed poor activity upon SDZ removal after a cycle with 120 min residence time, for both irradiated faces. Xiang et al. (Xiang. et al., 2021) and Liu et al. (2018) also evaluated the photocatalytic performance of TiO_2 in the degradation of SDZ and obtained similar results. The TiO_2/7.5 %-EG film exhibited the best photocatalytic activity under simulated sunlight, achieving 49.8 % steady-state SDZ degradation when the background face was irradiated, equivalent to a rate constant of 5.75×10^{-3} min^{-1}. The TiO_2/7.5 %-EG film showed pronounced surface modifications and large reduction in band gap energy when compared to pure TiO_2, therefore promoting the highest SDZ degradation rates among all films tested.

Valentina Silva et al. (2023) and Li et al. (2022a) also evaluated the photocatalytic behavior of the TiO_2/C heterostructured photocatalysts in the degradation of SDZ. The authors observed that the addition of carbon considerably improved the efficiency of the composite photocatalyst, favoring the red-shifted photons absorption. The exfoliated graphite has a dual function in the composite photocatalyst: to keep the Ti^{3+} ions in the TiO_2 matrix, and to promote the formation of the semiconductor-C heterojunction by the Ti–C and Ti–*O*–C bonds (Štengl et al., 2011). This behavior enables the hybridization of the C2p and O2p orbitals, promoting the formation of intermediate energy levels between the valence band (VB) and conduction band (CB) of TiO_2 (C1s and O2p-C2p), which favors the narrowing of the band gap region (Tismanar et al., 2021; Jia et al., 2016; Serrano-Luján et al., 2019), as observe from

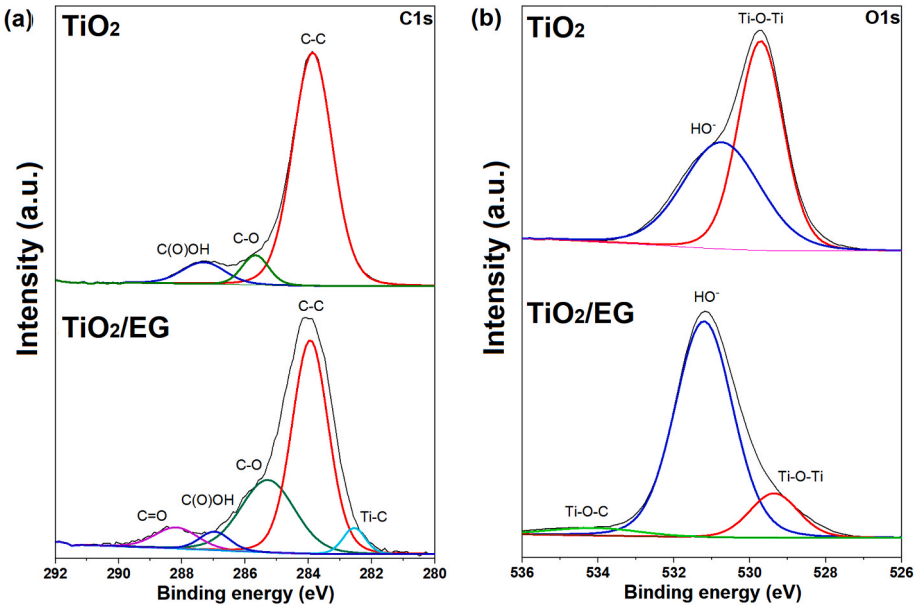

Fig. 6. High-resolution XPS spectra of the (a) C1s region and (b) O1s region, along with deconvoluted curves for the TiO_2 and TiO_2/EG films.

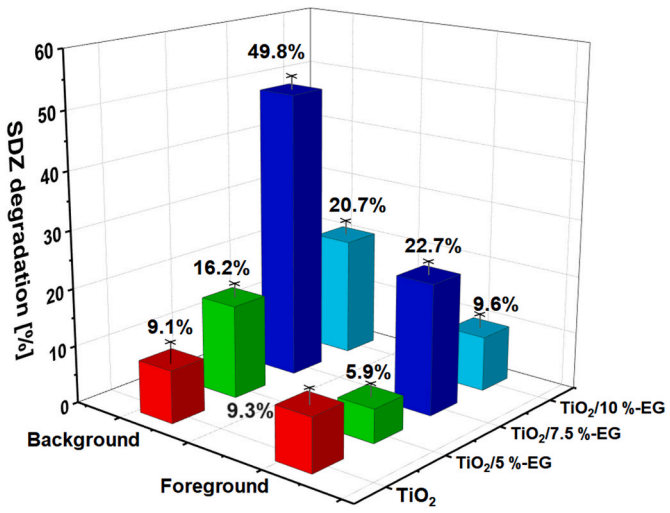

Fig. 7. Photocatalytic performance of TiO_2 and TiO_2/EG films in the degradation of sulfadiazine under UV–Vis irradiation.

Table 2
Photoactivity of the TiO_2 and TiO_2/EG films, with different carbon contents, under UV–Vis irradiation. The effect of irradiation mode on photocatalytic efficiency was evaluated by foreground and background irradiation (Fig. 1).

	Foreground (surface)		Background (substrate)	
	Degradation (%)	Rate constant (min^{-1})	Degradation (%)	Rate constant (min^{-1})
TiO_2	9.3 ± 2.1	(8.2 ± 1.9) × 10^{-4}	9.1 ± 1.7	(7.9 ± 1.5) × 10^{-4}
TiO_2/5 % - EG	5.9 ± 1.4	(5.1 ± 1.6) × 10^{-4}	16.2 ± 1.1	(1.5 ± 1.4) × 10^{-3}
TiO_2/7.5 % - EG	22.7 ± 1.9	(2.2 ± 2.1) × 10^{-3}	49.8 ± 1.3	(5.8 ± 1.1) × 10^{-3}
TiO_2/10 % - EG	9.6 ± 1.3	(8.4 ± 1.1) × 10^{-4}	20.7 ± 1.2	(1.9 ± 1.7) × 10^{-3}

the characterization results. Electrons (e^-) can be excited from VB to the C1s energy level, as well as can be promoted from hybridized O2p-C2p orbitals to CB. As a result, the electronic transition from the O2p-C2p energy level to C1s can also occur, and more electrons (e^-) can effectively participate in photocatalytic reactions (Eqs. (4)–(6)), resulting in increased photocatalytic performance.

$$e^- + > Ti^{IV}OH \rightarrow > Ti^{III}OH \quad (4)$$

$$> Ti^{III}OH\,(e^-) + EG(e^-) + O_2 \rightarrow O_2^{\bullet -} \quad (5)$$

$$O_2^{\bullet -} + HO^{\bullet} + SDZ \rightarrow CO_2 + H_2O + \text{inorganic species} \quad (6)$$

The investigation also suggests that the irradiation pathways influence the photocatalytic performance. As shown in Fig. 7 and Table 2, when the TiO_2/7.5 %-EG film was irradiated from the foreground (surface), its photocatalytic efficiency was 22.7 %. Nevertheless, when the respective composite film was irradiated from the background (substrate), its photocatalytic efficiency was increased to 49.8 %. A similar behavior was observed for TiO_2/5 %-EG and TiO_2/10 %-EG films, with an improvement from 5.9 % to 16.2 % and from 9.6 % to 20.7 %, respectively. Few studies have been reported on the effect of irradiation pathways on continuous photocatalytic reactors, most of them on background irradiation. Cen et al. (2006) evaluated the effect of background irradiation on photocatalytic efficiencies of TiO_2 thin films. When compared with foreground irradiation, background irradiation can avoid the loss of light energy in the solution, which was also observed in the present research. The possible UV–Vis photocatalytic mechanism of the irradiation mode effect is proposed in Fig. 8.

In the foreground irradiation mechanism (Fig. 8a), photons penetrate the glass window and the solution layer of about 1.6 mm before reaching the TiO_2/EG film. Consequently, the photocatalytic hybrid film suffers a severe loss of efficiency. Furthermore, the light transmittance through the SDZ solution decreases, even when keeping the visible light intensity constant (Xiang. et al., 2021). SDZ molecules may absorb an amount of visible light irradiation necessary to TiO_2/EG surface activation, which can reduce the photocatalytic efficiency. In the background irradiation (Fig. 8b), light transmits directly to the photocatalyst material and suffers little loss, which results in a high photocatalytic efficiency. Then, the film absorbs the photons and electron (e^-)/hole (h^+) pairs are photogenerated. Superoxide ($O_2^{\bullet -}$) and hydroxyl ($HO^{\bullet}$) radicals are formed and promote the oxidation of the adsorbed pollutant molecules to complete the photocatalytic reaction (Reza et al., 2017; Palharim et al., 2022; Zhang et al., 2022; Marcello et al., 2020). Peng et al. (2017) and Ma et al. (2001) also reported that the photocatalytic rate of the background irradiation mode was much higher than that of the foreground irradiation mode. Relevant studies have also evaluated the photocatalytic behavior of visible light active composite photocatalysts immobilized on glass substrates (Castillo et al., 2023; Valadez-Renteria et al., 2023; Castillo and Rodríguez-González, 2022). The authors observed similar results to those found here. In addition to high degradation efficiency under visible light, the possibility of reuse of the photocatalysts was also noted.

3.6.1. *Reusability tests*

The reusability of the photocatalytic films is an important requirement for its practical applications in water treatment. Therefore, the TiO_2/7.5 %-EG film was subjected to SDZ degradation for four cycles with 120 min of residence time each, resulting in a total of 480 min of simulated solar radiation on the background face. As shown in Fig. 9, after four photocatalytic cycles a reduction from 49.8 % to 40.3 % in the photocatalytic activity of TiO_2/7.5 %-EG films was observed; a similar trend was observed in previous investigations (Bento et al., 2021a; Marcello et al., 2020; Ismail et al., 2013). Liu et al. (2018) suggested that low initial SDZ concentration favors the degradation rate. Nevertheless, higher SDZ concentrations, can impregnate the TiO_2/EG surface and slow down photocatalytic degradation (Liu et al., 2017). The observed saturation can be associated to intermediate products adsorbed on the surface of the films (Liu et al., 2018; Bel Hadjltaief et al., 2013). The obtained results support that the TiO_2/EG composite films synthetized by the proposed method can be applied in practice to water treatment for antibiotic removal under sunlight.

3.6.2. *Investigation of the role of oxidizing species in the photocatalytic behavior of TiO_2/EG films*

Additional tests were performed with radical scavengers and with the TiO_2/7.5 %-EG film obtained by airbrush spray coating (Fig. 10). The inhibition of SDZ degradation was: 90.8 % with sodium azide >83.6 % with KI > 70.2 % with TBA >41.9 % with 1,4-hydroquinone >30.4 % with formic acid. Sodium azide is generally used to scavenge e^-, but it is also a good scavenger of $^{\bullet}OH$ radicals (Schneider et al., 2020; Palharim et al., 2024). During photocatalytic reactions, e^- react with oxygen to generate $O_2^{\bullet -}$ radicals, which can react with SDZ molecules; thus, the strong inhibition of SDZ degradation observed when sodium azide was used may indicate that fewer $O_2^{\bullet -}$ radicals were formed. Since iodine donates electrons to holes in the valence band of the semiconductor, KI is applied to scavenge h^+, although it can also quench $^{\bullet}OH$ radicals (Schneider et al., 2020). TBA, in turn, reacts very well with $HO^{\bullet}$, (k = 4.2-7.6 × 10^8 L mol^{-1} s^{-1}) (Lee and Tang, 1982; Gordon et al., 1977), while 1,4-hydroquinone can scavenge both $HO^{\bullet}$ radicals ($k = 2.1 \times 10^{10}$ L mol^{-1} s^{-1}) and $O_2^{\bullet -}$ ($k = 1.6 \times 10^7$ L mol^{-1} s^{-1}) (Fónagy et al., 2021). Finally, formic acid is a good h^+ scavenger (Schneider et al., 2020; Pelaez et al., 2016), but it can also react with $HO^{\bullet}$, with a high-rate constant (k = 1.2 × 10^8 L mol^{-1} s^{-1}) (Buxton, 1988). In this context,

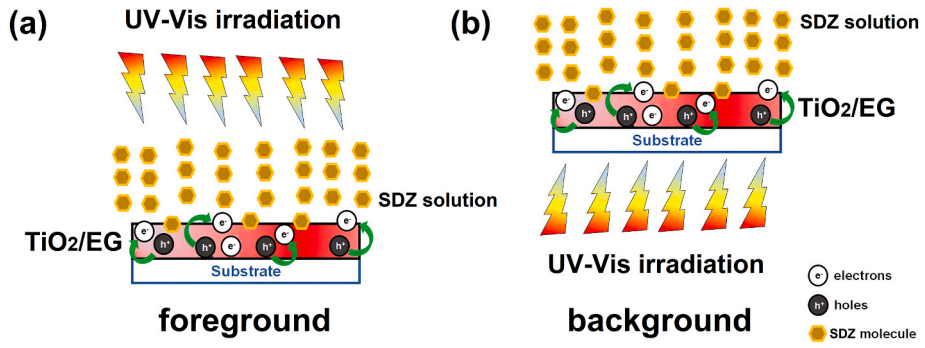

Fig. 8. Scheme of the proposed UV–Vis photocatalytic mechanism for the (a) foreground and (b) background irradiation effect for the 300-nm-thick TiO_2/EG composite films deposited on borosilicate glass substrates by the airbrush spray coating method.

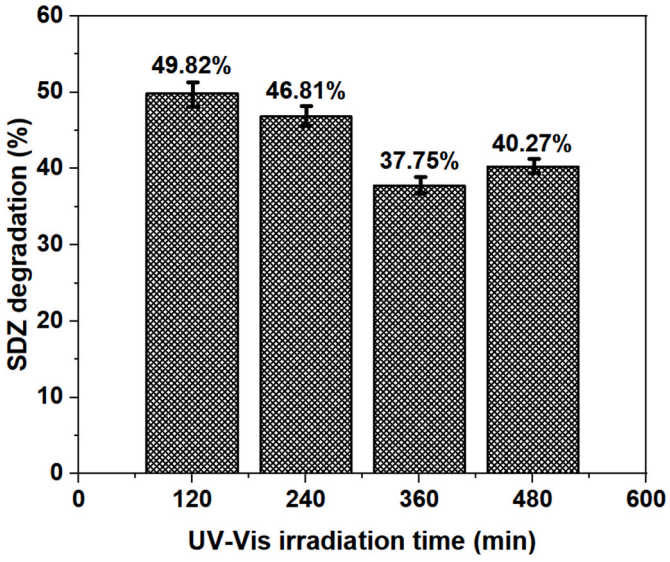

Fig. 9. Reusability of TiO_2/7.5 %-EG film for the photocatalytic degradation of sulfadiazine under UV–Vis irradiation over 480 min. Standard deviation around ±2 %.

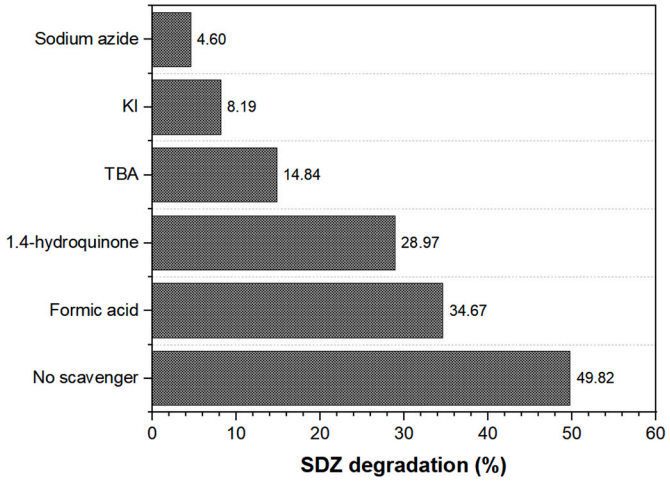

Fig. 10. Effect of scavengers on the photocatalytic behavior of the TiO_2/7.5%-EG film.

these results indicate that $HO^{\bullet}$, $O_2^{\bullet-}$, and h^+ are the main oxidizing species involved in the degradation of SDZ.

The valence band (E_{VB}) and conduction band (E_{CB}) potential energies of the composite photocatalysts was estimated from Eqs. (7) and (8), where X is the absolute electronegativity of the semiconductor (5.82 eV for TiO_2) (Bai et al., 2021); E^e is the free electron energy (4.5 eV); and E_g is the band gap energy (TiO_2 = 3.2 eV; TiO_2/EG = 2.1 eV), as shown in Fig. 5.

$$E_{VB} = X - E^e + 0.5E_g \quad (7)$$

$$E_{CB} = E_{VB} - E_g \quad (8)$$

The estimated energy potentials for the TiO_2 film were E_{VB} = 2.9 eV and E_{CB} = −0.3 eV, while for the TiO_2/EG film the values of E_{VB} and E_{CB} were 2.37 eV and 0.27 eV, respectively. Fig. 11 shows the proposed photocatalytic mechanism for the TiO_2/EG composite films under UV–Vis irradiation. The expanded graphite can act as a p-type semiconductor, with E_g = 2.2 eV and energy potential of the CB at −0.5 eV. In this process, the photogenerated electrons (e^-) in the CB of expanded graphite transfer freely to the CB of TiO_2, enhance the reduction of the Ti^{4+} cations to Ti^{3+} ions (Eq. (4)), and react with the SDZ molecules and dissolved oxygen. Electrons (e^-) participate in the reduction of O_2, which results in the formation of superoxide radical ions $O_2^{\bullet-}$ (Eq. (5)). The holes (h^+) from the VB of TiO_2 migrate to expanded graphite, which facilitates the spatial separation of the photogenerated electronic pairs, and minimizes recombination, promoting the formation of more oxidizing species. CB potential of the EG is relatively more negative than the CB potential of TiO_2.This behavior is characteristic of a type-II heterojunction (Murugan et al., 2021; Tang et al., 2018; Jia et al., 2016). The results suggest that the expanded graphite promoted significant changes in the electronic structure of the photocatalysts, which improved their performance under UV–Vis irradiation.

The possible degradation pathways of SDZ by UV–Vis-active TiO_2/EG composite photocatalysts can be elucidated from the reaction process of hydroxylation, desulfonation, denitrification, oxidation and cleavage (Xiang. et al., 2021; Li et al., 2022b). Initially, $O_2^{\bullet-}$ and $HO^{\bullet}$ species reacts with sulfonamide group on the end of S atom, which can break the C–N and C═N bonds of the pyrimidine ring (Liu et al., 2018). The γ-cleavage by oxidizing species attack can form 2-sulfamic acid pyrimidine (Xiang. et al., 2021). Cleaved S–N and C–S sites may promote the other intermediates formation, such as *p*-aminobenzenesulfonic acid ($C_6H_7NO_3S$), 2-aminopyrimidine ($C_4H_5N_3$), and aniline (C_6H_7N) (Liu et al., 2018; Xu et al., 2023; Baran et al., 2009). Overall, the obtained results indicate that TiO_2/EG supported photocatalysts represent a potential approach for real environmental applications in sunlight-based water treatment.

4. Conclusions

TiO_2 films and TiO_2/expanded graphite composite films were successfully synthetized by sol-gel process and deposited by airbrush spray coating technique. The results allow to conclude.

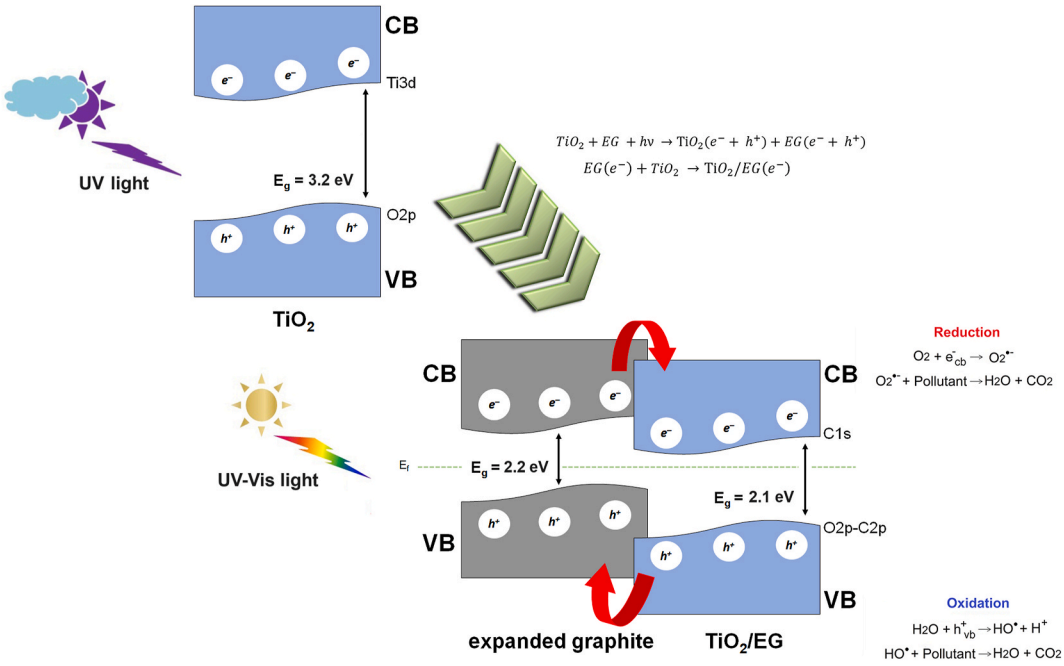

Fig. 11. Demonstrative scheme of the proposed photocatalytic mechanism for the UV–Vis active TiO_2/EG composite photocatalyst.

- The addition of EG nanosheets promoted important morphological modifications and changes in the electronic structure of the hybrid films and type-II heterojunction was observed;
- TiO_2/EG composite films exhibit good photocatalytic behavior, with efficiency around 49.8 % for the TiO_2/7.5 %-EG in sulfadiazine degradation. Background irradiation mode showed better photocatalytic performance than foreground irradiation possibly due to the transmittance of light to the photocatalyst. A possible irradiation pathway mechanism was proposed.
- Durability experiments revealed the possibility of practical use of the composite films after 480 min. The results suggest that TiO_2/EG photocatalysts obtained by spray coating represent a viable option for real photocatalytic applications in sunlight-based water treatment.

CRediT authorship contribution statement

Rodrigo Teixeira Bento: Writing – original draft, Software, Methodology, Investigation, Data curation, Conceptualization. **Priscila Hasse Palharim:** Writing – original draft, Software, Investigation, Formal analysis, Data curation. **Antonio Carlos Silva Costa Teixeira:** Writing – review & editing, Supervision, Resources, Project administration, Funding acquisition. **Marina Fuser Pillis:** Writing – review & editing, Visualization, Validation, Supervision, Resources, Project administration, Funding acquisition, Formal analysis.

Declaration of competing interest

The authors declare that they have no known competing financial interests or personal relationships that could have appeared to influence the work reported in this paper.

Data availability

No data was used for the research described in the article.

Acknowledgments

The authors are grateful to the Brazilian agencies CNPq (National Council for Scientific and Technological Development, grants No. 168935/2018-0, 311230/2020-2, and 420135/2023-5) and FAPESP (São Paulo Research Foundation, grants No. 2019/24158-9 and 2018/21271-6); to Escola Politécnica, University of São Paulo (Department of Electrical Engineering) for the Raman spectroscopy and UV–Vis spectrophotometry assays; and to UFABC (Federal University of ABC) for the XPS assays.

References

Akhavan, O., Ghaderi, E., 2009. Photocatalytic reduction of graphene oxide nanosheets on TiO_2 thin film for photoinactivation of bacteria in solar light irradiation. J. Phys. Chem. C 113, 20214–20220. https://doi.org/10.1021/jp906325q.

Ali, T., Mohyuddin, S., Ali, G., Ibrar, M., Summer, F., Iqbal, S., Xie, Y., Maqbool, M., 2022. Synthesis of graphite doped TiO_2 nanotubes, and their structural, electronic, and photocatalytic characterization, Electron. Mater. Lett. 18, 69–78. https://doi.org/10.1007/s13391-021-00317-5.

Aouf, D., Henni, A., Selloum, D., Khane, Y., Fenniche, F., Zerrouki, D., Belkhalfa, H., Dizge, N., 2023. Facile preparation and characterization of nanostructured ZnS/PbS heterojunction thin films for enhanced microbial inhibition and photocatalytic degradation. Mater. Chem. Phys. 295, 127059 https://doi.org/10.1016/j.matchemphys.2022.127059.

Bai, N., Liu, X., Li, Z., Ke, X., Zhang, K., Wu, Q., 2021. High-efficiency TiO_2/ZnO composites photocatalysts by sol-gel and hydrothermal methods. J. Sol. Gel Sci. Technol. 99, 92–100. https://doi.org/10.1007/s10971-021-05552-8.

Baran, W., Adamek, E., Sobczak, A., Sochacka, J., 2009. The comparison of photocatalytic activity of Fe-salts, TiO_2 and TiO_2/$FeCl_3$ during the sulfanilamide degradation process. Catal. Commun. 10, 811–814. https://doi.org/10.1016/j.catcom.2008.12.026.

Bel Hadjltaief, H., Da Costa, P., Galvez, M.E., Ben Zina, M., 2013. Influence of operational parameters in the heterogeneous photo-Fenton discoloration of wastewaters in the presence of an iron-pillared clay. Ind. Eng. Chem. Res. 52, 16656–16665. https://doi.org/10.1021/ie4018258.

Bento, R.T., Correa, O.V., Pillis, M.F., 2019. Photocatalytic activity of undoped and sulfur-doped TiO_2 films grown by MOCVD for water treatment under visible light. J. Eur. Ceram. Soc. 39, 3498–3504. https://doi.org/10.1016/j.jeurceramsoc.2019.02.046.

Bento, R.T., Correa, O.V., Pillis, M.F., 2021a. On the surface chemistry and the reuse of sulfur-doped TiO_2 films as photocatalysts. Mater. Chem. Phys. 261, 124231 https://doi.org/10.1016/j.matchemphys.2021.124231.

Bento, R.T., Correa, O.V., Antunes, R.A., Pillis, M.F., 2021b. Surface properties enhancement by sulfur-doping on TiO_2 films. Mater. Res. Bull. 143, 111460 https://doi.org/10.1016/j.materresbull.2021.111460.

Bento, R.T., Correa, O.V., Gastelois, P.L., Pillis, M.F., 2022. VIS-active TiO_2 films decorated by expanded graphite: impact of the exfoliation time on the photocatalytic behavior. Environ. Technol. 44, 29. https://doi.org/10.1080/09593330.2022.2163708.

Buxton, G.V., 1988. Critical Review of rate constants for reactions of hydrated electrons, hydrogen atoms and hydroxyl radicals (OH/·O− in Aqueous Solution. J. Phys. Chem. Ref. Data 17, 513. https://doi.org/10.1063/1.555805.

Castillo, P.C.H.D., Rodríguez-González, V., 2022. Efficient visible photocatalytic degradation of 4-CP herbicide using immobilized TiO_2:Ni on glass substrates. Top. Catal. 65, 1139–1148. https://doi.org/10.1007/s11244-022-01679-2.

Castillo, P.C.H.D., Robledo-Trujillo, G., Rodríguez-González, V., 2023. Development of a visible-light-active-$NiTiO_3$ coating for the efficient removal of the persistent herbicide 2,6-dichlorobenzamide (BAM) from drinking water. Chemosphere 339, 139628. https://doi.org/10.1016/j.chemosphere.2023.139628.

Cen, J., Li, X., He, M., Zheng, S., Feng, M., 2006. The effect of background irradiation on photocatalytic efficiencies of TiO_2 thin films. Chemosphere 62, 810–816. https://doi.org/10.1016/j.chemosphere.2005.05.008.

De Araujo Gusmão, C., Palharim, P.H., Ramos, B., Teixeira, A.C.S.C., 2022. Enhancing the visible-light photoactivity of silica-supported TiO_2 for the photocatalytic treatment of pharmaceuticals in water. Environ. Sci. Pollut. Res. 29, 42215–42230. https://doi.org/10.1007/s11356-021-16718-w.

Duoerkun, G., Zhang, Y., Shi, Z., Shen, X., Cao, W., Liu, T., Liu, J., Chen, Q., Zhang, L., 2020. Construction of n-TiO_2/p-Ag_2O junction on carbon fiber cloth with Vis–NIR photoresponse as a filter-membrane-shaped photocatalyst. Adv. Fiber Mater. 2, 13–23. https://doi.org/10.1007/s42765-019-00025-8.

Fónagy, O., Szabó-Bárdos, E., Horváth, O., 2021. 1,4-Benzoquinone and 1,4-hydroquinone based determination of electron and superoxide radical formed in heterogeneous photocatalytic systems. J. Photochem. Photobiol. Chem. 407, 113057 https://doi.org/10.1016/j.jphotochem.2020.113057.

Gordon, S., Schmidt, K.H., Hart, E.J., 1977. A pulse radiolysis study of aqueous benzene solutions. J. Phys. Chem. 81, 104–109. https://doi.org/10.1021/j100517a003.

Guan, S., Hao, L., Yoshida, H., Itoi, T., Asanuma, H., Pan, F., Lu, Y., 2016. Fabrication and characterization of photocatalyst composite coatings of TiO_2/TiC-Ti using Ti and TiC powders. Surf. Coat. Technol. 307, 627–632. https://doi.org/10.1016/j.surfcoat.2016.09.038.

Guan, S., Cheng, Y., Hao, L., Yoshida, H., Tarashima, C., Zhan, T., Itoi, T., Qiu, T., Lu, Y., 2023. Oxygen vacancies induced band gap narrowing for efficient visible-light response in carbon-doped TiO_2. Sci. Rep. 13, 14105 https://doi.org/10.1038/s41598-023-39523-6.

Gueymard, C.A., 2004. The sun's total and spectral irradiance for solar energy applications and solar radiation models. Sol. Energy 76 (4), 423–453. https://doi.org/10.1016/j.solener.2003.08.039.

Ismail, A.A., Geioushy, R.A., Bouzid, H., Al-Sayari, S.A., Alhajry, A., Bahnemann, D.W., 2013. TiO_2 decoration of graphene layers for highly efficient photocatalyst: impact of calcination at different gas atmosphere on photocatalytic efficiency. Appl. Catal. B: Environm. 129, 62–70. https://doi.org/10.1016/j.apcatb.2012.09.024.

Jia, J., Li, D., Wan, J., Yu, X., 2016. Characterization and mechanism analysis of graphite/C-doped TiO_2 composite for enhanced photocatalytic performance. J. Ind. Eng. Chem. 33, 162–169. https://doi.org/10.1016/j.jiec.2015.09.030.

Jiang, B., Tian, C., Zhou, W., Wang, J., Xie, Y., Pan, Q., Ren, Z., Dong, Y., Fu, D., Han, J., Fu, H., 2011. In situ growth of TiO_2 in interlayers of expanded graphite for the fabrication of TiO_2-graphene with enhanced photocatalytic activity. Chem. Europ. J. 17, 8379–8387. https://doi.org/10.1002/chem.201100250.

Karthik, P., Gowthaman, P., Venkatachalam, M., Rajamanickam, A.T., 2020. Propose of high performance resistive type H_2S and CO_2 gas sensing response of reduced graphene oxide/titanium oxide (rGO/TiO_2) hybrid sensors. J. Mater. Sci. Mater. Electron. 31, 3695–3705. https://doi.org/10.1007/s10854-020-02928-4.

Khalid, N.R., Bilal Tahir, M., Majid, A., Ahamed, E., Ahmad, M., Khalid, S., Ahmed, W., 2018. TiO_2-graphene-based composites: synthesis, characterization, and application in photocatalysis of organic pollutants. Micro and Nanomanufacturing 2, 95–122. https://doi.org/10.1007/978-3-319-67132-1_5.

Lastre-Acosta, A.M., Cruz-González, G., Nuevas-Paz, L., Jáuregui-Haza, U.J., Teixeira, A.C.S.C., 2015. Ultrasonic degradation of sulfadiazine in aqueous solutions. Environ. Sci. Pollut. Res. 22, 918–925. https://doi.org/10.1007/s11356-014-2766-2.

Lastre-Acosta, A.M., Cristofoli, B.S., Parizi, M.P.S., Do Nascimento, C.A.O., Teixeira, A.C.S.C., 2021. Photochemical persistence of sulfa drugs in aqueous medium: kinetic study and mathematical simulations. Environ. Sci. Pollut. Res. 28, 23887–23895. https://doi.org/10.1007/s11356-020-11715-x.

Lee, J.H., Tang, I.N., 1982. Absolute rate constants for the hydroxyl radical reactions with ethane, furan, and thiophene at room temperature. J. Chem. Phys. 77, 4459. https://doi.org/10.1063/1.444367.

Levenspiel, O., 2013. The Chemical Reactor Omnibook. Lulu Press, Morrisville, NC, USA.

Li, X., Shen, R., Ma, S., Chen, X., Xie, J., 2018. Graphene-based heterojunction photocatalysts. Appl. Surf. Sci. 430, 53–107. https://doi.org/10.1016/j.apsusc.2017.08.194.

Li, Q., Huang, Y., Pan, Z., Ni, J., Yang, W., Chen, J., Zhang, Y., Li, J., Hollow, C., 2022a. N-TiO_2@C surface molecularly imprinted microspheres with visible light photocatalytic regeneration availability for targeted degradation of sulfadiazine. Sep. Purif. Technol. 299 https://doi.org/10.1016/j.seppur.2022.121814.

Li, Q., Huang, Y., Pan, Z., Ni, J., Yang, W., Chen, J., Zhang, Y., Li, J., 2022b. Hollow C, N-TiO_2@C surface molecularly imprinted microspheres with visible light photocatalytic regeneration availability for targeted degradation of sulfadiazine. Separ. Purif. Technol. 299, 121814 https://doi.org/10.1016/j.seppur.2022.121814.

Li, D., Li, R., Zhou, D., Qin, X., Yan, W., 2023. S–scheme TiO_2/ZnS heterojunction as dual-reaction sites: a high–efficiency and spontaneous photocatalyst for hydrogen production under light irradiation. Vacuum 210, 111906. https://doi.org/10.1016/j.vacuum.2023.111906.

Liu, B., Zhao, X., Zhao, Q., He, X., Feng, J., 2005. Effect of heat treatment on the UV-vis-NIR and PL spectra of TiO_2 films. J. Electron Spectrosc. Related Phenom. 148, 158–163. https://doi.org/10.1016/j.elspec.2005.05.003.

Liu, X., Cong, R., Cao, L., Liu, S., Cui, H., 2014. The structure, morphology and photocatalytic activity of graphene-TiO_2 multilayer films and charge transfer at the interface. New J. Chem. 38, 2362–2367. https://doi.org/10.1039/C3NJ01003A.

Liu, Y., Jin, W., Zhao, Y., Zhang, G., Zhang, W., 2017. Enhanced catalytic degradation of methylene blue by α-Fe_2O_3/graphene oxide via heterogeneous photo-Fenton reactions. Appl. Catal. B Environ. 206, 642–652. https://doi.org/10.1016/j.apcatb.2017.01.075.

Liu, X., Liu, Y., Lu, S., Guo, W., Xi, B., 2018. Performance and mechanism into TiO_2/Zeolite composites for sulfadiazine adsorption and photodegradation. Chem. Eng. J. 350, 131–147. https://doi.org/10.1016/j.cej.2018.05.141.

Ma, Y., Qiu, J.B., Cao, Y.A., Guan, Z., Yao, J., 2001. Photocatalytic activity of TiO_2 films grown on different substrates. Chemosphere 44, 1087–1092. https://doi.org/10.1016/S0045-6535(00)00360-X.

Marcello, B.A., Correa, O.V., Bento, R.T., Pillis, M.F., 2020. Effect of growth parameters on the photocatalytic performance of TiO_2 films prepared by MOCVD. J. Braz. Chem. Soc. 31, 1270–1283. https://doi.org/10.21577/0103-5053.20200012.

Murugan, C., Ranjithkumar, K., Pandikumar, A., 2021. Interfacial charge dynamics in type-II heterostructured sulfur doped-graphitic carbon nitride/bismuth tungstate as competent photoelectrocatalytic water splitting photoanode. J. Colloid Interf. Sci. 602, 437–451. https://doi.org/10.1016/j.jcis.2021.05.179.

Palharim, P.H., Fusari, B.L.D.R., Ramos, B., Otubo, L., Teixeira, A.C.S.C., 2022. Effect of HCl and HNO_3 on the synthesis of pure and silver-based WO_3 for improved photocatalytic activity under sunlight. J. Photochem. Photobiol. Chem. 422, 113550 https://doi.org/10.1016/j.jphotochem.2021.113550.

Palharim, P.H., Gusmão, C., Ramos, B., Bento, R.T., Pillis, M.F., Teixeira, A.C.S.C., 2024. Highly stable WO_3-Ag-AgCl films for continuous water treatment synthesized using a new low-cost ultrasonic spray pyrolysis/photoreduction approach. J. Environm. Chem. Eng. 12, 112895 https://doi.org/10.1016/j.jece.2024.112895.

Pelaez, M., Falaras, P., Likodimos, V., O'Shea, K., De La Cruz, A.A., Dunlop, P.S.M., Byrne, J.A., Dionysiou, D.D., 2016. Use of selected scavengers for the determination of NF-TiO_2 reactive oxygen species during the degradation of microcystin-LR under visible light irradiation. J. Molec. Catal. A. Chem. 425, 183–189. https://doi.org/10.1016/j.molcata.2016.09.035.

Peng, Z., Liu, X., Lin, G., 2017. The synergistic degreasing treatment of background irradiated photocatalysis and microreactor. Catal. Commun. 90, 79–82. https://doi.org/10.1016/j.catcom.2016.11.008.

Ramos, B., Carneiro, J.G.M., Nagamati, L.I., Teixeira, A.C.S.C., 2021. Development of intensified flat-plate packed-bed solar reactors for heterogeneous photocatalysis, Environment. Sci. Pollut. Res. 28, 24023–24033. https://doi.org/10.1007/s11356-020-11806-9.

Reza, K.M., Kurny, A.S.W., Gulshan, F., 2017. Parameters affecting the photocatalytic degradation of dyes using TiO_2: a review. Appl. Water Sci. 7, 1569–1578. https://doi.org/10.1007/s13201-015-0367-y.

Rivas-Ortiz, I.B., Cruz-González, G., Lastre-Acosta, A.M., Manduca-Artiles, M., Rapado-Paneque, M., Chávez-Ardanza, A., Teixeira, A.C.S.C., Jáuregui-Haza, U.J., 2017. Optimization of radiolytic degradation of sulfadiazine by combining Fenton and gamma irradiation processes. J. Radioanal. Nucl. Chem. 314, 2597–2607. https://doi.org/10.1007/s10967-017-5629-8.

Samet, L., Ben Nasseur, J., Chtourou, R., March, K., Stephan, O., 2013. Heat treatment effect on the physical properties of cobalt doped TiO_2 sol-gel materials. Mater. Character 85, 1–12. https://doi.org/10.1016/j.matchar.2013.08.007.

Schneider, J.T., Firak, D.S., Ribeiro, R.R., Peralta-Zamora, P., 2020. Use of scavenger agents in heterogeneous photocatalysis: truths, half-truths, and misinterpretations. Phys. Chem. Chem. Phys. 22, 15723–15733. https://doi.org/10.1039/d0cp02411b.

Serrano-Luján, L., Víctor-Román, S., Toledo, C., Sanahujaparejo, O., Mansour, A.E., Abad, J., Amassian, A., Benito, A.M., Maser, W.K., Urbina, A., 2019. Environmental impact of the production of graphene oxide and reduced graphene oxide. SN Applied Science 1, 179. https://doi.org/10.1007/s42452-019-0193-1.

Silva, V., Fernandes, J.F.A., Tomás, M.C., Silva, C.P., Calisto, V., Otero, M., Lima, D.L.D., 2023. Enhanced solar driven photocatalytic removal of antibiotics from aquaculture effluents by TiO_2/carbon quantum dot composites. Catal. Today 419, 114150. https://doi.org/10.1016/j.cattod.2023.114150.

Štengl, V., Popelková, D., Vlácil, P., 2011. TiO_2-graphene composite as high performance photocatalysts. J. Phys. Chem. C 115, 25209–25218. https://doi.org/10.1021/jp207515z.

Sun, J., Zhang, H., Guo, L.H., Zhao, L.X., 2013. Two-dimensional interface engineering of a titania-graphene nanosheet composite for improved photocatalytic activity, ACS App. Mater. Interf. 5, 13035–13041. https://doi.org/10.1021/am403937y.

Tang, B., Chen, H., Peng, H., Wang, Z., Huang, W., 2018. Graphene modified TiO_2 composite photocatalysts: mechanism, progress and perspective. Nanomaterials 8, 105. https://doi.org/10.3390/nano8020105.

Temam, E.G., Djani, F., Rahmane, S., Temam, H.B., Gasmi, B., 2022. Photocatalytic activity of Al/Ni doped TiO_2 films synthesized by sol-gel method: dependence on thickness and crystal growth of photocatalysts. Surface. Interfac. 31, 102077 https://doi.org/10.1016/j.surfin.2022.102077.

Tismanar, I., Obreja, A.C., Buiu, O., Duta, A., 2021. VIS-active TiO_2-graphene oxide composite thin films for photocatalytic applications. App. Surf. Sci. 538, 147833 https://doi.org/10.1016/j.apsusc.2020.147833.

Valadez-Renteria, E., Perez-Gonzalez, R., Gomez-Solis, C., Diaz-Torres, L.A., Encinas, A., Oliva, J., Rodriguez-Gonzalez, V., 2023. A novel and stretchable carbon-nanotube/Ni@TiO_2:W photocatalytic composite for the complete removal of diclofenac drug from the drinking water. J. Environm. Sci. 126, 575–589. https://doi.org/10.1016/j.jes.2022.05.028.

Vallejo, W., Rueda, A., Díaz-Uribe, C., Grande, C., Quintana, P., 2019. Photocatalytic activity of graphene oxide-TiO_2 thin films sensitized by natural dyes extracted from

Bactris guineensis. Royal Soc. Open Sci. 6, 181824 https://doi.org/10.1098/rsos.181824.

Wannapop, S., Somdee, A., 2022. Highly orientated one-dimensional Cu_2O/TiO_2 heterostructure thin film for photoelectrochemical photoanode and photocatalytic degradation applications. Thin Solid Films 747, 139144. https://doi.org/10.1016/j.tsf.2022.139144.

Wu, F., Liu, W., Qiu, J., Li, J., Zhou, W., Fang, Y., Zhang, S., Li, X., 2015. Enhanced photocatalytic degradation and adsorption of methylene blue via TiO_2 nanocrystals supported on graphene-like bamboo charcoal. Appl. Surf. Sci. 358, 425–435. https://doi.org/10.1016/j.apsusc.2015.08.161.

Wu, R., Li, L., Zhang, N., He, J., Song, L., Zhang, G., Zhang, Z., He, H., 2021. Enhancement of low-temperature NH_3-SCR catalytic activity and H_2O & SO_2 resistance over commercial V_2O_5-MoO_3/TiO_2 catalyst by high shear-induced doping of expanded graphite. Catal. Today 376, 302–310. https://doi.org/10.1016/j.cattod.2020.04.051.

Xiang, X., Wu, L., Zhu, J., Li, J., Liao, X., Huang, H., Fan, J., Lv, K., 2021. Photocatalytic degradation of sulfadiazine in suspensions of TiO_2 nanosheets with exposed (001) facets. Chin. Chem. Lett. 32, 3215–3220. https://doi.org/10.1016/j.cclet.2021.03.064.

Xu, M., Yan, S., Liu, X., Sun, S., Khan, Z.U.H., Wu, W., Sun, J., 2023. Theoretical investigation on the degradation of sulfadiazine in water environments: oxidation of $^{\bullet}OH$, $SO_4^{\bullet-}$ and $CO_3^{\bullet-}$ and reactivity of $(TiO_2)_n$ clusters (n = 1–6). J. Environm. Chem. Eng. 11, 109994 https://doi.org/10.1016/j.jece.2023.109994.

Xue, B., Zou, Y., Yang, Y., 2017. A UV-light induced photochemical method for graphene oxide reduction. J. Mater. Sci. 52, 12742–12750. https://doi.org/10.1007/s10853-017-1266-4.

Zabihi, F., Ahmadian-Yazdi, M.-R., Eslamian, M., 2017. Photocatalytic graphene-TiO_2 thin films fabricated by low-temperature ultrasonic vibration-assisted spin and spray coating in a sol-gel process. Catalysts 7, 136. https://doi.org/10.3390/catal7050136.

Zhang, Y., Sun, T., Zhang, D., Shi, Z., Zhang, X., Li, C., Wang, L., Song, J., Lin, Q., 2020. Enhanced photodegradability of PVC plastics film by codoping nano-graphite and TiO_2. Polym. Degrad. Stabil. 181, 109332 https://doi.org/10.1016/j.polymdegradstab.2020.109332.

Zhang, X., Chen, H., Liu, S., Zhang, B., Zhu, H., Chen, H., Wen, B., Chen, L., 2022. Preparation of TiO_2-graphitized carbon composite photocatalyst and their degradation properties for tetracycline antibiotics. J. Molec. Struct. 1270, 133897 https://doi.org/10.1016/j.molstruc.2022.133897.